

A two-dimensional network simulator for two-phase flow in porous media

Eyvind Aker, Knut Jørgen Maløy
Department of Physics
University of Oslo, N-0316 Oslo, Norway

Alex Hansen
Department of Physics, Norwegian University of Science
and Technology, N-7034 Trondheim, Norway

G. George Batrouni
Institut Non-Linéaire de Nice,
Université de Nice – Sophia Antipolis, 06560 Valbonne, France

January 8, 2022

Abstract

We investigate a two-dimensional network simulator capable of modeling different time dependencies in two-phase drainage displacements. In particular, we focus on the temporal evolution of the pressure due to capillary and viscous forces and the time dependence of the interface between the two liquids. The dynamics of the capillary effect are taken into account and we report on high accuracy pressure measurements. Moreover, the simulator includes important features in drainage, like burst dynamics of the invading fluid and simultaneous flow of two liquids in a section of a tube. The validity of the model is checked by comparing simulation results with well known experimental properties in drainage displacement.

Also at: IKU Petroleum Research, N-7034 Trondheim, Norway

1 Introduction

Two-phase displacements in porous media have been much studied over the last two decades. The main reason for this is the great variety of structures observed when changing the physical parameters of the fluids like viscosity contrast, wettability, interfacial tension and displacement rate. Besides being a process of great interest in modern physics, it has a large number of practical applications in many fields of science like oil recovery and hydrology.

The main purpose of this paper is to present a network simulator modeling inmiscible two-phase flow on a two-dimensional lattice of cylindrical tubes. Primarily, the model is developed to measure the time dependence of different physical properties and to study the dynamics of the fluid movements. We focus on drainage displacements, i.e. the process where a non-wetting fluid displaces a wetting fluid in a porous medium. In particular, we report on the dynamics of the temporal evolution of the pressure due to capillary and viscous forces and the time dependence of the interface between the two liquids.

The different structures between the invading and the defending fluids obtained in drainage divide into three major flow regimes: viscous fingering [4,16], stable displacement [13] and capillary fingering [15]. There exist statistical models like DLA [22], anti-DLA [18] and invasion percolation [21] that reproduce the basic domains in viscous fingering, stable displacement and capillary fingering respectively. However, these models do not contain any physical time for the front evolution and they cannot describe the crossover between the major flow regimes.

To overcome the limitations of the statistical models several network simulators similar to the one presented in this paper, have been developed over the last two decades [2,4,6,11,13]. The different models are more or less simplified to avoid computational complications, and difficulties most often arise when the capillary effects are taken into account. Lenorm and et al. (1988) assigned each tube a threshold pressure and allowed the injecting non-wetting fluid to enter the tube only when the pressure exceeded the threshold value of that tube. Moreover, the non-wetting fluid was restricted to flow in the positive direction relative to the direction of the displacement. Dias and Payatakes (1986) suggested a more realistic approximation by introducing tubes with walls with a sinusoidal profile. They let the capillary pressure of the meniscus change as the menisci invaded the tubes.

Similar to the idea of Dias and Payatakes (1986) the model reported here

takes into account the capillary effects by letting the capillary pressure of the meniscus depend on its position inside the tube. Moreover, the menisci can both invade into or retreat from a tube. This is an important property in slow drainage, where the invading fluid is found to suddenly invade a larger region causing another part to retreat (bursts) [10,14,17]. Experiments performed by Malý et al. (1992) have also produced evidence that the bursts are characterized by large pressure fluctuations (Haines jumps). To measure these pressure fluctuations the flow field in our network simulator is solved for a constant injection rate rather than a constant pressure.

In the present model an approximation is developed to model a mixture of the wetting and non-wetting fluids when they flow simultaneously in a cross section of a tube. Such mixing is an important process in both drainage and imbibition [7,14] and should not be neglected. The piston-like motion characterizing slow drainage is well described, but additional mechanisms observed in imbibition [3,14] is not taken into account.

The paper is organized as follows. Section 2 describes the porous medium model used in the network simulator. Section 3 gives the solution of the flow field with the constraint of a constant injection rate, and Section 4 describes the algorithm for updating the menisci. In Section 5 we discuss how to move the menisci into neighboring tubes and allow mixing of the two liquids. Finally, in Section 6 we give some simulation results focusing on calibrations of the model. At the end some conclusions are discussed.

2 The Porous Medium Model

2.1 Geometry of Model Porous Medium

The porous medium is represented by a square lattice of tubes inclined 45 degrees. Thus, if all tubes are equal and a uniform pressure across the lattice is applied, a liquid flows equally well in tubes inclined to the left as tubes inclined to the right. The tubes are connected together at nodes, where four tubes meet. There is no volume assigned to the nodes: the tubes represent the volume of both pores and throats. The liquids flow from the bottom to the top of the lattice and periodic boundary conditions are applied horizontally. The pressure difference between the first (bottom of system) and the last (top) rows defines the pressure across the lattice. Gravity effects are neglected, and as a consequence we consider a horizontal flow in a two-dimensional network of tubes. See figure 1 for details.

The tubes are cylindrical with equal length d , and every tube is assigned a

radius r which is chosen at random in the interval $[r_1; r_2]$. The randomness of the radii represent the disorder of an ordinary porous medium and r_1 and r_2 define the width of the distribution of radii.

Initially, the system is filled with a defending fluid with viscosity μ_1 . The invading fluid with viscosity μ_2 is injected from the bottom row with a constant injection rate. Here we report on the study of drainage displacements, and so let the invading fluid be non-wetting and the defending fluid be wetting. We assume that the fluids are immiscible and that there is a well defined interface between the two phases. The curvature of this interface gives rise to a capillary pressure given by the interfacial tension σ . Moreover, we will treat the liquids as incompressible, i.e. the volume flux Q into the system must equal the volume flux Q out of the system.

2.2 Capillary Flow in a tube

Consider a tube containing a meniscus between nodes i and j in the network as shown in figure 2. The volume flux q_{ij} through the tube from the i th to the j th node is found from the Washburn equation for capillary flow [20]:

$$q_{ij} = \frac{r_{ij}^2 k_{ij}}{\mu_{eff}} \frac{1}{d} (p_{ij} - p_c) \quad (1)$$

Here $k_{ij} = r_{ij}^2$ is the permeability, $\mu_{eff} = \mu_2 x_{ij} + \mu_1 (1 - x_{ij})$ is the effective viscosity due to the two fluids, $p_{ij} = p_j - p_i$ is the pressure difference between the i th and j th node and $p_c = p_1 - p_2$ defines the capillary pressure. x_{ij} is the position of the meniscus in the tube and r_{ij} is the radius of the tube. The position of the meniscus is a continuous function in the range $[0; 1]$ and the flow direction is given by the sign of q_{ij} : When $q_{ij} > 0$ the fluids in the tube flow to the right, otherwise they flow to the left. As mentioned in the introduction, it is important to allow flow in both directions in order to study the dynamics when the menisci invade into or retreat from a tube.

For a tube without a meniscus present $p_c = 0$, and equation (1) reduces to that describing Hagen-Poiseuille flow.

The capillary pressure p_c due to the meniscus is given by the Young-Laplace law. Let θ refer to the wetting angle between the non-wetting and wetting phases as shown in figure 2. Then

$$p_c = \frac{2\sigma}{r} \cos \theta \quad (2)$$

where $r = \cos \theta$ is the principal radius of curvature of the meniscus. σ denotes the interfacial tension between the two phases.

Equation (2) is derived under the assumption that the fluids are in static equilibrium, i.e. $p_{ij} = p_c$. A more detailed description of the dynamics of a moving interface is still an open problem [8]. However, at low flow rates when no mixing or turbulence occur, we consider the above expression as a reasonable approximation.

A real porous medium consists of a complex network of throats and pores with a great variety of shapes. The curvature of a meniscus traveling in this network, becomes a continuous function depending on the meniscus' position. The variation in curvature results in local changes in the capillary pressure. Equation (2) does not take this effect into account, since the capillary pressure is assumed constant for each tube. Instead, we apply a dependency in p_c as a function of the meniscus' position inside each tube. Thus, we define the capillary pressure p_c as (without index notations):

$$p_c = \frac{2}{r} [\sigma \cos(2x)] ; \quad (3)$$

where we have assumed perfect wetting ($\theta = 0$). In the above formula r denotes the radius of the actual tube and x is the position of the meniscus in that tube. The function is plotted in figure 3. The definition sets the capillary pressure equal to zero at the ends of the tube whereas p_c becomes equal to the threshold pressure p_t when the meniscus is in the middle of the tube, i.e. $p_t = 4\sigma/r$. The threshold pressure is the minimum capillary pressure required to let the non-wetting fluid invade the tube.

3 Solving the Flow Field

The fluids are assumed incompressible leading to conservation of volume flux at each node:

$$\sum_j q_{ij} = 0 ; \quad (4)$$

Here q_{ij} denotes the flow through a tube connecting node i and j . Equation (4) is simply Kirchhoff's equation and in the summation j runs over the nearest neighbor nodes to the i th node. The index i runs over all nodes that do not belong to the top or bottom rows, that is, the internal nodes. This set of linear equations are to be solved with the constraint that the pressures at the nodes belonging to the upper and lower rows are kept fixed.

By inserting equation (1) in equation (4) we get:

$$\sum_j G_{ij} (p_j - p - p_c) = 0 ; \quad (5)$$

where G_{ij} defines the mobility of the tube, i.e. $G_{ij} = \frac{r_{ij}^2 k_{ij}}{4\eta l_{ij}} = \text{eff}$. In order to write this set of equations as a matrix equation, we move all the capillary pressures and the fixed pressure referring to the nodes belonging to the upper and lower rows to the right-hand side of equation (5). The matrix equation may then be written as

$$\sum_j D_{ij} p_j = B_i ; \quad (6)$$

where the indices i and j only run over internal nodes. D_{ij} are elements a conductance matrix D [1] where the elements depend on the connection between different tubes and their respective mobility. p_j are the elements in the pressure vector, containing the pressure at the internal nodes and B_i contains the pressure at the boundaries (upper and lower rows) and the capillary pressure if a meniscus is present in the tube.

We are seeking the solution of the pressure at the internal nodes for a given configuration of the menisci, i.e.

$$p_j = \sum_i (D^{-1})_{ij} B_i ; \quad (7)$$

This equation is solved by using the Conjugate Gradient method [1].

3.1 Solving for a Constant Injection Rate

The pressures solved by equation (7) correspond to keeping the applied pressure difference across the network constant. We want to study the dynamics of the pressure fluctuations at a constant displacement rate. Thus, we need to find the pressures p_j under constant injection rate of the invading fluid.

For two-phase displacement in a porous medium the injection rate Q is given by

$$Q = A P + B ; \quad (8)$$

Here P is the pressure across the lattice and A and B are parameters depending on the geometry of the medium and the current configuration of the liquids. The first part of equation (8) is simply Darcy's law for one phase

flow through a porous medium. The last part B results from the capillary pressure between the two phases. As long as the menisci are kept at fixed positions B becomes a constant.

The pressure across the lattice for a given injection rate is

$$P = \frac{Q}{A} + B ; \quad (9)$$

The parameters A and B are calculated by solving the pressure field (7) for two different pressures P^0 and P^∞ applied across the lattice. The obtained pressure vectors give the corresponding injection rates, Q^0 and Q^∞ . We are now in the position to calculate A and B by solving the set

$$Q^0 = A P^0 + B ; \quad (10)$$

$$Q^\infty = A P^\infty + B ; \quad (11)$$

The next step is to relate the internal pressures at the nodes to the constant injection rate. From equation (1) we can write the flow rate q_{ij} from node i to node j like

$$q_{ij} = a_{ij} p_{ij} + b_{ij} ; \quad (12)$$

where a_{ij} and b_{ij} are parameters depending on the permeability of the tube, the effective viscosity and the capillary pressure due to a meniscus. From equation (9) the pressure P for a given Q is found. Thus, we could proceed by solving Kirchhoff's equation with the constraint of applying this pressure at the inlet. That would give the correct flow rates in each tube for the desired Q . However, the following method will save a third solution of equation (7).

All the equations involved in the calculations are linear, i.e. they have the functional form $f(x) = ax + b$. As a consequence the pressure p_{ij} between node i and j becomes a linear function of the pressure P across the lattice:

$$p_{ij} = \alpha_{ij} P + \beta_{ij} ; \quad (13)$$

Here are α_{ij} and β_{ij} parameters depending on the configuration of the fluids. By inserting this into equation (12) and redefine a_{ij} 's and b_{ij} 's we obtain

$$q_{ij} = \mathbf{a}_{ij} P + \mathbf{b}_{ij} ; \quad (14)$$

The parameters \mathbf{a}_{ij} and \mathbf{b}_{ij} are found from the flow rates q_{ij}^0 and q_{ij}^∞ corresponding to the two pressures P^0 and P^∞ respectively. Note that the

parameters A and B in (8) and a_{ij} and B_{ij} in (14) all depend on the current position of the menisci and we therefore need to solve them for every new fluid configuration.

The solution due to a constant injection rate can now be summarized into two steps: (a) After we have found A and B we use equation (9) to get P for the desired Q . (b) This P is then used in equation (14) to get the local flow q_{ij} .

The validity of equation (13) is easily checked by solving Kirchhoff's equation for the calculated pressure P and compare the solution with the one given from equation (14). Numerical results show excellent agreement between these two solutions.

4 Updating the Menisci

A time step t is chosen such that every meniscus is allowed to travel at most a maximum step length x_{max} during that time step. This leads to the formula

$$t = \min_{ij} \frac{x_{max}}{v_{ij}} ; \quad (15)$$

where $v_{ij} = q_{ij} / r_{ij}^2$ denotes the flow velocity in a tube containing a meniscus between the i th and the j th node. The time step becomes dependent on the local velocity. This method is sometimes called event driven updating.

During the time step it is checked whether or not a meniscus crosses the middle or the end of a tube. If this happens, the time step is reduced such that only one meniscus reaches the end or the middle of the tube. A meniscus reaching the end of a tube is moved into the neighbor tubes (see section 5).

In the middle of the tube the capillary pressure becomes equal to the threshold pressure. At this point, the menisci in slow drainage are found to become unstable and suddenly invade the tube like a burst [10,14,17]. Often a cascade of bursts are released in rapid succession around the original instability, before a new stable position is reached. Moreover, the bursts are characterized by large pressure fluctuations [17]. It is important to detect the order in which the instabilities occur to ensure that the right path of least resistance is chosen. This is done by adjusting the time step when a meniscus approaches the middle of a tube such that the exact occurrence of the burst is detected.

The new positions of the menisci are calculated by using a second order Runge-Kutta scheme [19]. Numerical analysis from the present model shows that this scheme produces more stable solutions than the less accurate and more unstable Euler scheme. However, with an event driven time step as defined in equation (15), the implementation of the second order Runge-Kutta scheme is not straightforward. Before discussing our modifications, we first remind the reader of the Runge-Kutta scheme.

Let x_n denote the position of a meniscus at time t_n and let the next position at time $t_{n+1} = t_n + \tau$ be x_{n+1} where τ is the time step found from (15). The second order Runge-Kutta scheme then becomes [19]

$$x_{n+1} = x_n + k_2 + O(\tau^3); \quad (16)$$

$$k_1 = \tau v(t_n; x_n); \quad (17)$$

$$k_2 = \tau v(t_n + \frac{1}{2}\tau; x_n + \frac{1}{2}k_1); \quad (18)$$

where $v(t_n; x_n)$ denotes the local flow rate in each tube and $v(t_n + \frac{1}{2}\tau; x_n + \frac{1}{2}k_1) = v_{mid}(t_n; x_n)$ denotes the midpoint velocity.

Note that the velocities defining the time step in equation (15) correspond to the derivative of the curve x_n at the starting point of each time interval. I.e. $v(t_n; x_n) = v_{ij}$, where the subscript ij is omitted on the left hand side of the equality. When the menisci are updated by using the velocities $v(t_n; x_n)$, equation (15) leads to the condition

$$\dot{x}_{n+1} \leq x_{n+1} \leq x_{max}; \quad (19)$$

for all the menisci. In the second order Runge-Kutta scheme the next position x_{n+1} is found by using the midpoint velocity $v_{mid}(t_n; x_n)$, which in general differs from $v(t_n; x_n)$. As a consequence, condition (19) may no longer be valid and the displacement length or the stability of the numerical solution, are no longer controlled. Assume that the position of the menisci is a smooth function of time, the effect vanishes since $v_{mid}(t_n; x_n) \approx v(t_n; x_n)$. Moreover, there is no problem as long as $v_{mid}(t_n; x_n) \approx v(t_n; x_n)$. The problem arises when $v_{mid}(t_n; x_n) \neq v(t_n; x_n)$ and the total displacement becomes much larger than x_{max} . To avoid this scenario the time step is redefined by inserting the midpoint velocities in equation (15). A new midpoint velocity corresponding to the redefined time step is calculated and the positions are updated according to this time step by using the new midpoint velocity. The procedure is repeated until the displacements become close enough to the maximum step length x_{max} . Typically, the total displacement must

not be larger than about 10% increase of x_{max} . Otherwise, the numerical solution may diverge.

5 Motion of the Menisci at the Nodes

A tube partially filled with one of the liquids is allowed to have either one or two menisci leading to four different arrangements as shown in figure 5. The menisci can be situated at any position inside the tube and the corresponding effective viscosity and capillary pressure are calculated. The effective viscosity becomes the sum of the fraction of the wetting and non-wetting fluid inside the tube multiplied with their respective viscosities. The absolute value of the capillary pressure is given by equation (3), while its sign depends on whether the meniscus is pointing upwards like in figure 4 (a) or downwards like in figure 4 (b). The menisci are updated according to the determined time step Δt from the previous section, and their respective flow rates v_{ij} . The total time lapse is recorded before the flow field is solved for the new fluid configuration. Note that due to the incompressibility of the liquids the two menisci within the same tube in figure 4 (c) and (d) always move with equal velocities. Thus, the volumes of the wetting in (c) or the non-wetting in (d) are conserved.

When a meniscus reaches the end of a tube it is moved into the neighbor tubes according to some defined rules. These rules take care of the different fluid arrangements that can appear around the node. Basically, the non-wetting fluid can either invade into or retreat from the neighbor tubes as shown in figure 5 (a) and (b) respectively. In 5 (a) the non-wetting fluid approaches the node from below (drainage). When the meniscus has reached the end of the tube (position 1), it is removed and three new menisci are created at position 2 in the neighbor tubes (position 2). The distance is about 15% of the tube length d and it defines the node region where the capillary pressure is zero. The node region avoids that the created menisci at position 2 immediately disappear and move back to the initial position 1 in tubes where the flow direction is opposite to the direction of the invading fluid. The node region has also an important role that allows mixing of the liquids (see below).

Figure 5 (b) shows the opposite case when the non-wetting fluid retreats into a single tube (imbibition). As figure 5 shows the properties of imbibition should not be neglected as long as the menisci can travel in both directions. However, in drainage which is what we are focusing on, arrangement (b) will

appear rarely compared to (a).

When the menisci are moved a distance Δx into the neighbor tubes the total time lapse is adjusted due to the injection rate of the invading fluid. The adjustment is calibrated such that the amount of the invading fluid in the lattice always equals the injected volume. The injected volume is the product of the time lapse and the injection rate.

Difficulties arise when we want to create a new meniscus in a tube that already contains two menisci. To allow such movement the two original menisci and the new meniscus are merged into one by the following method. Consider a scenario like figure 5 (a) but assume now that the leftmost tube already contains a bubble of non-wetting fluid as shown in figure 6 (a). To merge the three menisci in the leftmost tube into one, we move the wetting fluid between position 2 and 3 to the left side of the non-wetting bubble and remove the menisci at position 2 and 3 before the meniscus at position 4 is moved to the right a distance equal to the original length between position 2 and 3 (figure 6 (b)). The same principles apply when the non-wetting fluid retreat into a tube that already contains a bubble of wetting fluid.

5.1 Mixing of the Fluids

The moving rules described in figure 5 and 6 solve the problem of modeling a "mixture" of the two liquids. Consider the situations shown in figure 7 where both the non-wetting and wetting fluids flow toward the node from the bottom and right tube respectively. Physically, it is expected that the fluid flowing out of the node is a mixture of both liquids. It is observed [7,14] that such simultaneous flow of both liquids in a tube takes place in so-called funicular continuous flow or a discontinuous dispersed flow. In the former case the wetting phase flows along the cylinder wall surrounding the non-wetting phase, which occupies the central portion of the tube. A discontinuous flow is characterized by a dispersed non-wetting phase flowing as isolated droplets in a continuous wetting phase.

A model describing funicular and dispersed flow would be too complicated. Instead, we assume that the simultaneous flow can be represented by a finite number of small bubbles of each liquid, placed next to each other inside the tube. By sorting the bubbles of same type of fluid they can be replaced by one or two menisci. The procedure is illustrated with an example in figure 7: When the meniscus in the bottom tube reaches the end of the tube it moves a distance Δx into the neighbor tubes (arrangements a and b). Due to the opposite flow direction in the right tube the created

meniscus in this tube flows back to the node (arrangement c) and moves into the neighbor tubes (arrangement d). Now, the new meniscus in the bottom tube again approaches the node from below (arrangement e) and creates a configuration with three menisci in the top and left tubes (arrangement f). To avoid that the number of menisci inside a single tube increases unchecked the three menisci at the top and the left tube are reduced to one by placing the wetting fluid on the top of the non-wetting one (arrangement g).

The reorganization when three menisci are reduced to one (figure 6 and 7) results in unphysical jumps in the capillary pressure. Due to the small size of the bubbles, the jumps usually appear as perturbations in the total pressure. A small number of such jumps will not affect the numerical solution very much. But, the moment they become more dominant the numerical solution may become unstable and diverge. We discuss this below.

6 Calibration of the Network Model

We present three different calibration simulations, one in each of the regimes of interest: viscous fingering, stable displacement and capillary fingering. The simulations are executed on a Cray T90 vector machine. The Conjugate Gradient method solving Kirchhoff's equations, is easy to vectorize and achieves high performance efficiency on vector machines. However, the amount of time required increases dramatically with the size of the lattice. For a lattice consisting of N tubes, the Conjugate Gradient method needs approximately N^2 iterations each time step to solve Kirchhoff's equations. Doubling the size of the lattice quadruples N , hence, the computation time increases by a factor of 16. In addition the number of the time steps before the invading fluid reaches the outlet strongly affects the CPU-time.

In two-phase fluid displacement there are mainly three types of forces: viscous forces in the invading fluid, viscous forces in the defending fluid and capillary forces due to the interface between them. This leads to two dimensionless numbers that can characterize the flow in porous media: the capillary number C_a and the viscosity ratio M .

The capillary number is a quantity describing the competition between capillary and viscous forces. It is defined as

$$C_a = \frac{Q}{\mu} ; \quad (20)$$

where Q (cm^2/s) denotes the injection rate, μ (Poise) is the maximum viscosity of the two fluids, A (cm^2) is the cross section of the inlet and

(dyn/cm) is the interfacial tension between the two phases. γ is the product of the length of the inlet and the mean thickness of the lattice due to the average radius of the tubes.

M defines the ratio of the viscosities of the two fluids and is given by the invading viscosity μ_2 divided with the defending viscosity μ_1 :

$$M = \frac{\mu_2}{\mu_1} :$$

The three simulations are performed with parameters as close as possible to the corresponding experiments done by Malý et al. (1985) and Frette et al. (1997). In light of that, the length d of all tubes in the lattices are set equal to 1 mm. Furthermore, the radii of the tubes are chosen randomly in the interval $0.05d < r < d$. The interfacial tension is set to $\gamma = 30$ dyn/cm and the viscosities of the defending and the invading fluids varies between 0.01 P ("water") and 10 P ("glycerol").

6.1 Viscous Fingering

Figure 8 shows the result of a simulation in the regime of viscous fingering performed on a lattice of 60 × 80 nodes. The corresponding pressure across the lattice as a function of time is shown in figure 9. The simulation is stopped at breakthrough of the invading non-wetting fluid. The displacements are done with a high injection rate, $Q = 1.5$ ml/m in and the invading fluid is less viscous than the defending wetting fluid, $\mu_2 = 0.010$ P and $\mu_1 = 10$ P. The capillary number and the viscosity ratio becomes $Ca = 4.6 \cdot 10^3$ and $M = 1.0 \cdot 10^3$ respectively.

In viscous fingering the principal force is due to the viscous forces in the defending fluid and the capillary forces at the menisci are less dominant. The pattern formation (figure 8) shows that the invading fluid creates typical fingers into the defending fluid.

The pressure across the lattice (figure 9) decreases as the less viscous fluid invades the system. Roughly, the pressure appears to decrease linearly as a function of time. However, the slope is non-trivial and results from the fractal development of the fingers. In addition to the fractal growth, the rate of change in the pressure depends on the viscosity contrast M between the two phases. The rapid decrease at the end of the pressure function corresponds to the breakthrough of the invading fluid at the outlet.

Figure 9 shows that there are small fluctuations in the average decreasing pressure function. The fluctuations correspond to the changes in the

capillary pressure as a meniscus invades into or retreats from a tube. The fluctuations are small compared to the total pressure and thus the capillary pressure cannot affect the result very much.

In addition to containing important physics, the pressure function in figure 9 is used to establish the stability and convergence properties of the numerical solution. For all simulations it is verified that this function converges towards a unique solution when $x_{max} = 0.1d$ and the menisci are updated according to the second order Runge-Kutta method as described in section 4. That means Kirchhoff's equation must be solved approximately 10-20 times to let a meniscus pass through a single tube. This is probably what we can expect when we want to measure the fluctuations in the pressure due to local capillary changes inside the tubes. With larger step lengths the variations in the capillary pressure are lost and the solution is no longer suitable for our measurements.

6.2 Stable Displacement

Figure 10 shows the result of a simulation performed in the regime of stable displacement on a lattice of 60 × 60 nodes. Figure 11 shows the corresponding pressure across the lattice as a function of time. The simulation is stopped when the invading fluid has about half filled the system. As in the case of viscous fingering $Q = 1.5 \text{ ml/m in}$ and $C_a = 4.6 \cdot 10^3$. The viscosities are $\eta_1 = 0.10 \text{ P}$ and $\eta_2 = 10 \text{ P}$ giving $M = 1.0 \cdot 10^4$. Thus, the invading non-wetting fluid is more viscous than the defending wetting fluid.

The fluid movements are dominated by the viscous forces in the invading liquid and like viscous fingering the capillary effects are negligible. The invading fluid generates a compact pattern with an almost flat front between the non-wetting and wetting fluid. The simulation is stopped after the width of the front has stabilized, that means after the width of the front stops growing.

The average pressure across the lattice (figure 11) increases according to the amount of the high viscosity invading fluid injected into the system. Due to the low viscosity defending fluid the pressure corresponds to the pressure across the invading phase and a linear increase in the pressure is observed after the front has stabilized. (In figure 11: $t > 50 \text{ s}$). Like in viscous fingering, the average slope of the pressure function also depends on the viscosity ratio M and the injection rate.

The viscous forces dominate the pressure evolution, but fluctuations due to capillary effects are observed. The perturbations have about the same size

as for viscous fingering, which is not surprising since the size distribution of the radii of the tubes is the same for the two cases. The threshold pressure setting the strength of the capillary fluctuations, is inversely proportional to the radius of the tubes.

In fast displacement the viscous forces are strong enough to deform and even move small regions of trapped defending fluid which are left behind the front. It is also observed that the invading fluid grows along the whole front, causing the corresponding menisci to reach the end of the tube approximately at the same time. All together the result is a lot of bubbles of non-wetting and wetting fluid which travel through the network. Physically, the bubbles are expected but at the time they become too dominant in the displacement they cause some computational complication. The bubbles increase the number of tubes that should contain three menisci. Thus, a large number of reorganizations inside the tubes are applied to fulfill the constraint of at most two menisci in each tube. Typically, this is observed in figure 11 where the fluctuations in last part of the pressure function seem to increase in amplitude. The increasing amplitude is a result of the unphysical pressure jumps when three menisci are reorganized into one. For that reason the simulation is stopped before breakthrough of the invading fluid.

Another shortcoming in fast displacement is that the effective time step may approach zero. When the bubbles develop the number of menisci increases causing many of them to arrive at the end of the tubes approximately at the same time. The result is that the difference of the arrival times for the menisci goes to zero and a lot of iterations are required to move the whole front further on. Numerical experiments have shown that the problem first arises when the displacement is rather fast, that means $C_a > 5 \cdot 10^3$.

6.3 The Regime of Capillary Fingering

Finally a calibration simulation is run in the regime of capillary fingering. The resulting pattern is shown in figure 12, and in figure 13 the corresponding pressure across the lattice as a function of time is plotted. The simulation is performed on a lattice of 40×60 nodes and the run is stopped when the invading fluid reaches the outlet. The two fluids have equal viscosities, $\eta_1 = \eta_2 = 0.50 P$, corresponding to similar experiments performed by Frette et al. (1997). The invading non-wetting fluid displaces the defending wetting fluid with a rather low injection rate, $Q = 0.20 \text{ ml/m in}$. The capillary number and the viscosity ratio become $C_a = 4.6 \cdot 10^6$ and $M = 1.0$

respectively.

In capillary fingering the displacement is so slow that the viscous forces are negligible, with the consequence that the main force is the capillary one between the two fluids. Only the strength of the threshold pressure in the tubes decides if the invading fluid invades that tube or not. Since the radii of the tubes (which determine the threshold pressures) are randomly chosen from a given interval, the non-wetting fluid follows a random path of least resistance.

Figure 12 shows a typical rough front between the invading and the defending fluids with trapped clusters of defending fluid left behind the front. As opposed to stable displacement the clusters appear at all sizes between the tube length and the maximum width of the front.

The pressure across the lattice (figure 13) exhibits sudden jumps according to the capillary variation when the non-wetting fluid invades (or retreats) a tube. The fluctuations identify the bursts where the invading fluid proceeds abruptly. An enlargement of a small part of the pressure function at a time around 550 s is given in figure 14. The figure shows clearly this kind of dynamics. The pressure across the lattice slowly increases in stable periods before the threshold pressure in the tube which is going to be invaded is reached. At the threshold pressure the meniscus becomes unstable and the invasion of fluid takes place in a burst accompanied by sudden negative jumps in the pressure. The pressure curve in figure 14 is in good qualitative agreement with experimental results [17].

The main problem in capillary fingering is the computation time. The above simulation used about 36 CPU hours at a Cray T90, on a smaller lattice than the ones for viscous fingering and stable displacements. The two latter cases required both about 7 CPU hours. The reason for this dramatic increase in computation time is explained by looking at the physical properties of capillary fingering. The invasion occurs in bursts and each burst is localized to some very few tubes. That means that even with step lengths equal to those of stable displacement the amount of invading fluid injected into the system each time step is much less. Now, compared to viscous fingering the total saturation of the invading fluid is relatively high and as a consequence, an enormous number of time steps are required to reach breakthrough. In the above simulation approximately 300,000 time steps are applied, while in the case of viscous fingering only about 2,500 steps were necessary to reach breakthrough.

7 Conclusions

We have presented and discussed a two-dimensional network model simulating drainage displacement. Moreover, we have performed numerical calibration simulations whose results are found to be in good qualitative agreement with the properties observed in the three major flow regimes: viscous fingering, stable displacement and capillary fingering.

An important feature of the model is the capability to study temporal evolutions of different physical properties taking place in the displacement process. This continues the work of understanding two-phase flow in porous media. In particular, we have presented calculations of the pressure evolutions where the dynamics of the capillary effects were taken into account. With the proposed model it is also possible to measure the viscous and capillary contribution to the total pressure. This is a great advance since corresponding measurements in experimental setups are too difficult. A quantification of the competition between viscous and capillary forces will help to characterize the different flow regimes observed in drainage displacement.

An approximation has been developed to simulate a simultaneous flow of the two liquids inside a single tube. The presented moving rules take care of this kind of mixing and actually, they are essential to make the model work. So far the moving rules are based on the mechanisms observed in drainage, but in principle it should be possible by a certain modifications to model imbibition as well.

The lattice sizes are limited by the computation time and the model requires usage of high performance vector machines. To afford simulations on lattice sizes comparable to those in experimental setups [9,16], more sophisticated and efficient algorithms have to be developed. Especially, vector machines with parallel capabilities should be considered.

Acknowledgments

We thank S. Basak, I.O. Frette and J. Schmittbuhl for valuable comments. The computations were done at HLRZ, Forschungszentrum Jülich GmbH and E.A. is grateful for the hospitality shown there. The work has received support from NFR, The Research Council of Norway.

References

- [1] Batrouni, G . G . and Hansen, A .: 1988, Fourier Acceleration of Iterative Processes in Disordered Systems, *J. Stat. Phys.* 52, pp. 747{773.
- [2] Blunt, M . and King, P .: 1990, Macroscopic parameters from simulations of pore scale flow, *Phys. Rev. A* 42, pp. 4780{4787.
- [3] Cieplak, M . and Robbins, M . O .: 1988, Dynamical Transition in Quasi-static Fluid Invasion in Porous Media, *Phys. Rev. Lett.* 60, pp. 2042{2045.
- [4] Chen, J.-D . and Wilkinson, D .: 1985 Pore-Scale Viscous Fingering in Porous Media, *Phys. Rev. Lett.* 55, pp. 1892{1895.
- [5] Constantinides, G . N . and Payatakes, A . C .: 1996, Network Simulation of Steady-State Two-Phase Flow in Consolidated Porous Media, *AIChE J* 42, pp. 369{382.
- [6] Dias, M . M . and Payatakes, A . C .: 1986, Network models for two-phase flow in porous media. Part 1. Immiscible micro-displacement of non-wetting fluids, *J. Fluid Mech.* 164, pp. 305{336.
- [7] Dullien F A L .: 1992 Porous media: fluid transport and pore structure, Academic Press, California, USA, pp. 333{336.
- [8] Dussen V, E . B .: 1979 On the spreading of liquids on solid surfaces: static and dynamic contact lines, *Ann. Rev. Fluid Mech.* 11, pp. 371{400
- [9] Frette, O . I., Mal y, K . J., Schmittbuhl, J. and Hansen, A .: 1997 Immiscible Displacement of Viscosity Matched Fluids In Two-Dimensional Porous Media, *Phys. Rev. E* . 55, pp. 2969{2975.
- [10] Haines, W . B .: 1930, Studies in the physical properties of soil, *J. Agr. Sci.* 20, pp. 97{116.
- [11] King, P . R .: 1987, The fractal nature of viscous fingering in porous media, *J. Phys. A* 20, pp. L529{L534.
- [12] Koplík, J. and Lasseter, T . J .: February 1985, Two-Phase Flow in Random Network Models of Porous Media, *Soc. Petr. Eng. J.*

- [13] Lenormand, R., Touboul, E. and Zarcone, C.: 1988, Numerical models and experiments on immiscible displacements in porous media, *J. Fluid Mech.* 189, pp. 165{187.
- [14] Lenormand, R. and Zarcone, C.: 1983, Mechanism of the displacement of one fluid by another in a network of capillary ducts, *J. Fluid Mech.* 135, pp. 337{353.
- [15] Lenormand, R. and Zarcone, C.: 1985, Invasion percolation in an etched network: measurement of a fractal dimension, *Phys. Rev. Lett.* 54, pp. 2226{2229.
- [16] Malý, K. J., Feder, J. and Jossang, T.: 1985, Viscous fingering fractals in porous media, *Phys. Rev. Lett.* 55, pp. 2688{2691.
- [17] Malý, K. J. and Funberg, L. and Feder, J. and Jossang, T.: 1992, Dynamics of slow drainage in porous media, *Phys. Rev. Lett.* 68, pp. 2161{2164.
- [18] Paterson, L.: 1984, Diffusion-limited aggregation and two-fluid displacements in porous media. *Phys. Rev. Lett.* 52, pp. 1621{1624.
- [19] Press, W. H. and Teukolsky, S. A. and Vetterling, W. T. and Flannery, B. P.: 1992, Numerical Recipes, Cambridge University Press, New York, USA, pp. 704{708.
- [20] Washburn, E. W.: 1921, The Dynamics of Capillary Flow, *Phys. Rev.* 17, pp. 273{283.
- [21] Wilkinson, D. and Wilkinson, J. F.: 1983, Invasion percolation: A new form of percolation theory, *J. Phys. A* 16, pp. 3365{3376.
- [22] Witten, T. A. and Sander, L. M.: 1981, Diffusion-limited aggregation, a kinetic critical phenomenon, *Phys. Rev. Lett.* 47, pp. 1400{1403.

Figure 1: A square lattice of tubes connected together at nodes. The size of the lattice is 10×10 nodes. The black region indicates the invading non-wetting fluid coming from below and the light gray indicates the defending wetting fluid flowing out of the top.

Figure 2: Flow in a tube containing a meniscus.

Figure 3: The capillary pressure p_c as a function of the meniscus' position x in that tube. In the middle of the tube at $x = d/2$ the capillary pressure becomes equal to the threshold pressure p_t .

Figure 4: Four different fluid arrangements inside one tube. The shaded and the white regions indicate the non-wetting and wetting fluid respectively.

Figure 5: The motion of the menisci at the nodes. (a): The non-wetting fluid (shaded) reaches the end of the tube (position 1) and is moved a distance into the neighbor tubes (position 2). (b): The wetting fluid (white) reaches the end of the tubes (position 1) and the non-wetting fluid (shaded) retreat to position 2. For both (a) and (b) a proper time is recorded due to the small movement.

Figure 6: Reduction of three menisci into one. (a): The non-wetting fluid has reached the end of the tube (position 1) and is going to be moved into the neighbor tubes (position 2). The three menisci in the left tube are reorganized causing the situation shown in (b) to appear. In the figures the arrows denote the length of the wetting fluid between position 2 and 3 which is equal to the distance the meniscus at position 4 is moved to the right.

Figure 7: A "mixture" of non-wetting (shaded) and wetting (white) which flow into the neighbor tubes. The different arrangements (a)-(g) are a result of applying the rules which are described earlier in this section. For all figures the fluids flow towards the node from the bottom and right tube while the fluids in the top and the left tube flow away from it (denoted by the arrows in (a)).

Figure 8: The pattern obtained of a simulation in the regime of viscous fingering on a lattice of 60×80 nodes. $C_a = 4:6 \cdot 10^3$ and $M = 1:0 \cdot 10^3$. The invading non-wetting fluid (black) displaces the defending wetting fluid (gray) from below. The simulation took about $7\frac{1}{2}$ hours on a Cray T90 vector machine.

Figure 9: The calculated pressure across the lattice as a function of time for viscous fingering. The pressure decreases with time due to the viscous forces in the defending fluid and the flow velocities of the moving finger tips. The perturbations correspond to the capillary forces due to the moving menisci. The time is the total time lapse required to let the invading fluid reach the outlet.

Figure 10: The pattern obtained of a simulation performed on a lattice of 60×60 nodes in the regime of stable displacement. $C_a = 4.6 \times 10^3$ and $M = 1.0 \times 10^4$. The invading non-wetting fluid (black) displaces the defending wetting fluid (gray) from below. The simulation took about 7 hours on a Cray T90 vector machine.

Figure 11: The calculated pressure across the lattice as a function of time for stable displacement. For $t > 50$ s the pressure increases linearly with time due to the viscous forces in the invading fluid and the constant injection rate. The perturbations correspond to the capillary forces along the front.

Figure 12: The pattern obtained of a simulation performed on a lattice of 40×60 nodes in the regime of capillary fingering. $C_a = 4.6 \times 10^3$ and $M = 1.0 \times 10^4$. The invading non-wetting fluid (black) displaces the defending wetting fluid (gray) from below. The simulation took about 36 hours on a Cray T90 vector machine.

Figure 13: The calculated pressure across the lattice as a function of time for capillary fingering. The fluctuations due to the capillary forces correspond to the burst dynamics of the invading fluid. See also figure 14.

Figure 14: A magnification of the pressure across the lattice as a function of time in the interval 540-560 s. The fluid invasion takes place in bursts characterized by the negative pressure jumps.

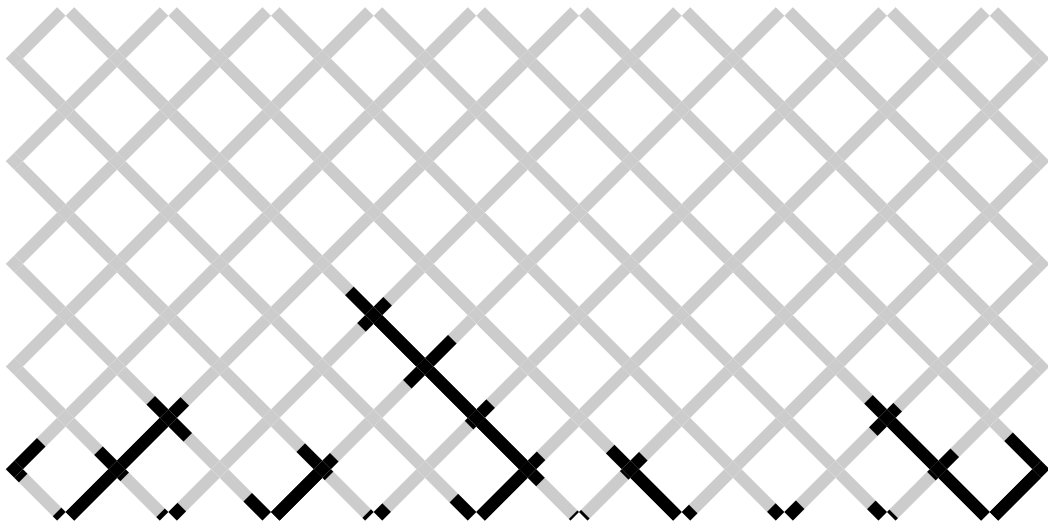


Figure 1

Aker et al.

Network Simulator for...

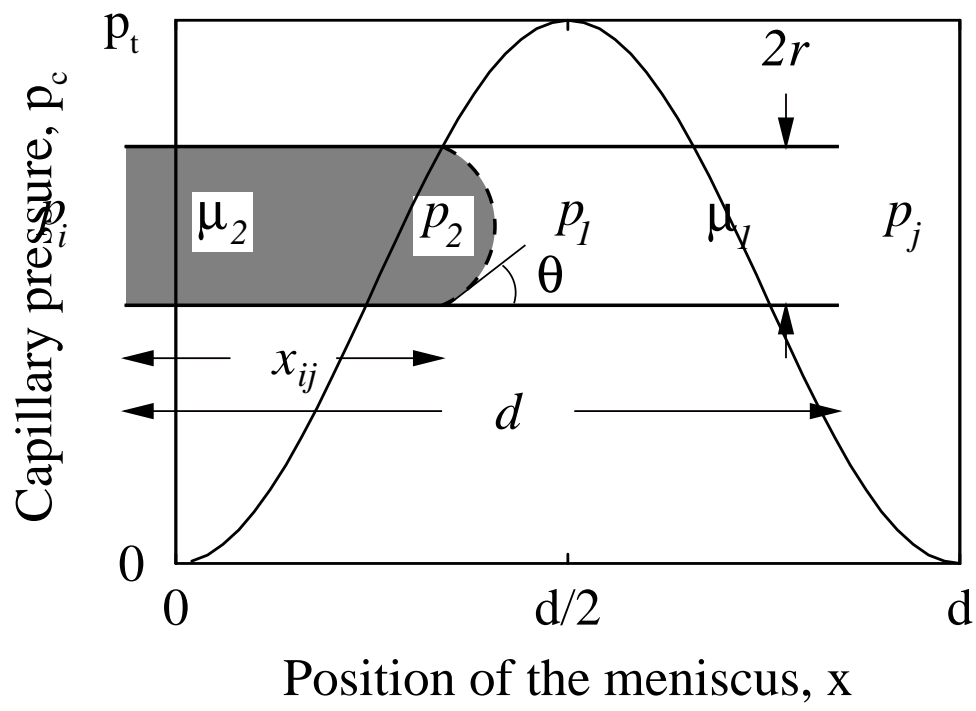


Figure 3

Aker et al.

Network Simulator for...

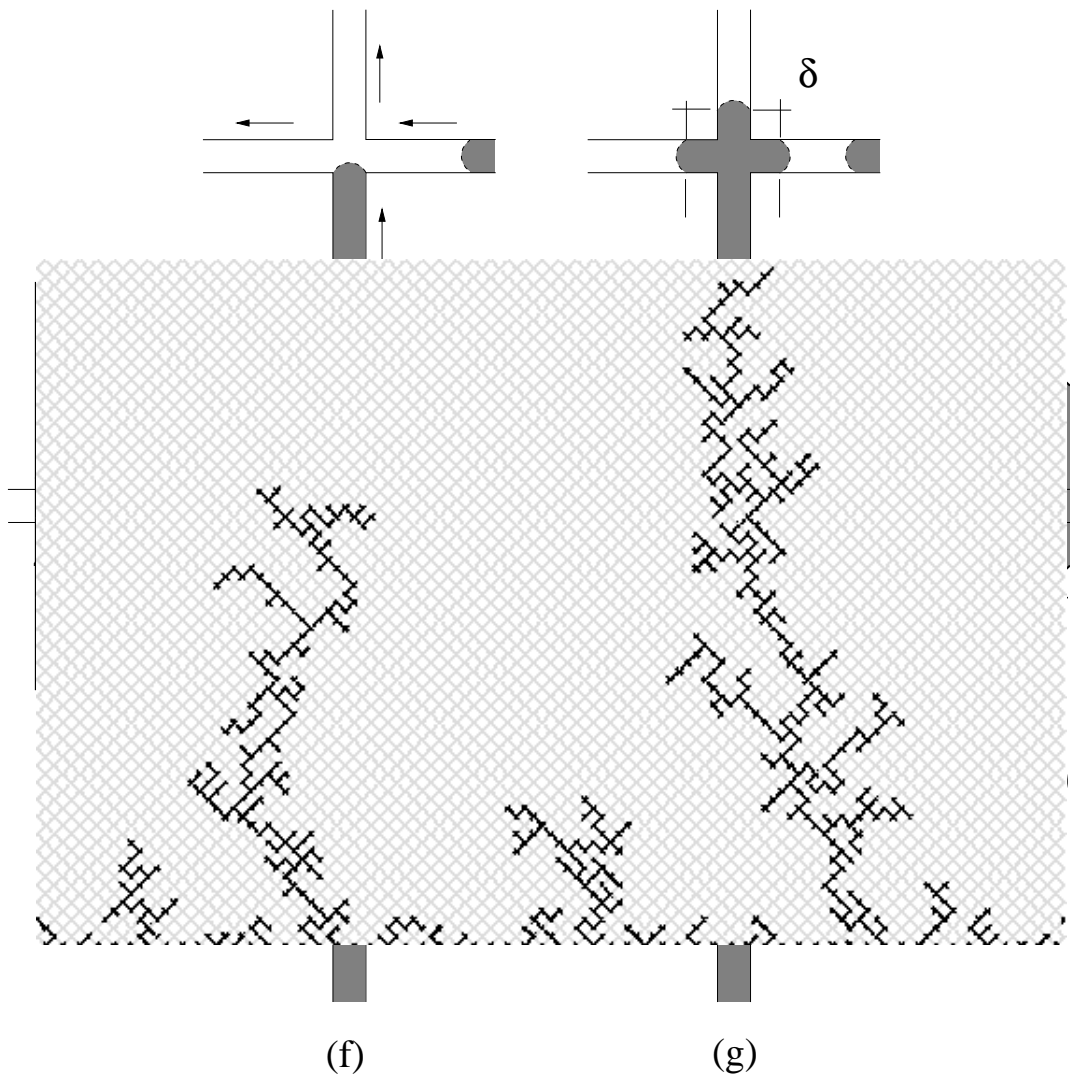


Figure 5

Aker et al.

Network Simulator for...

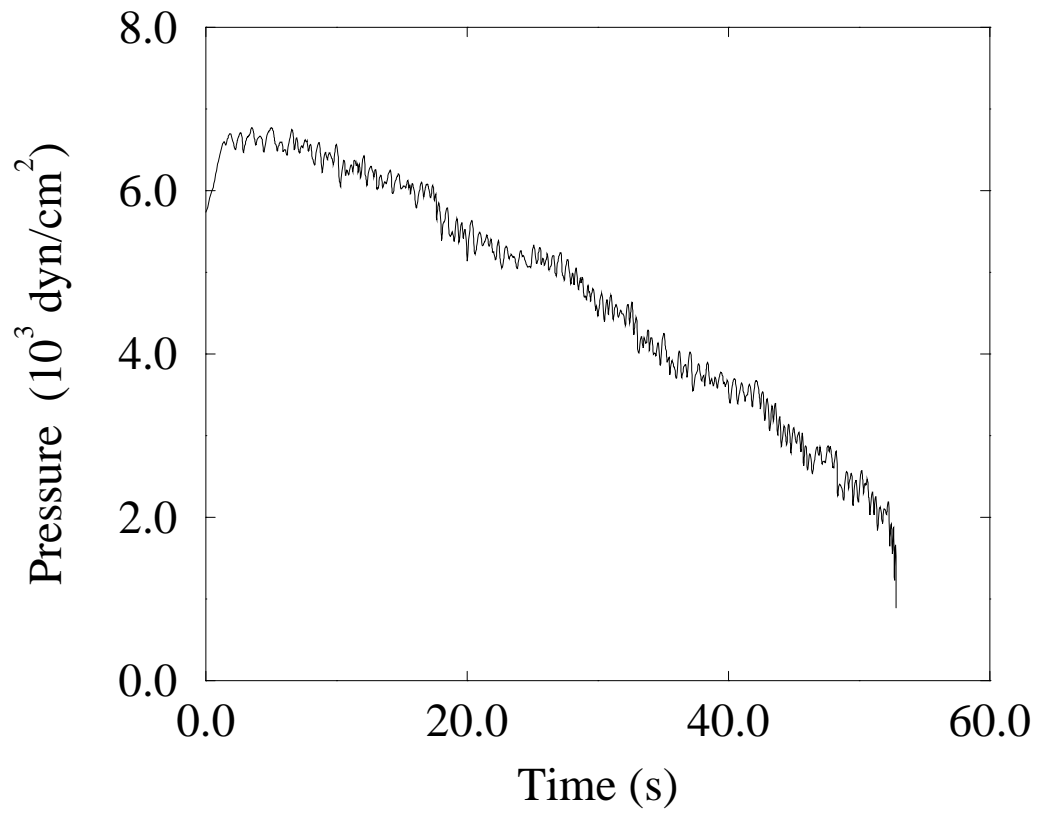


Figure 9

Aker et al.

Network Simulator for...

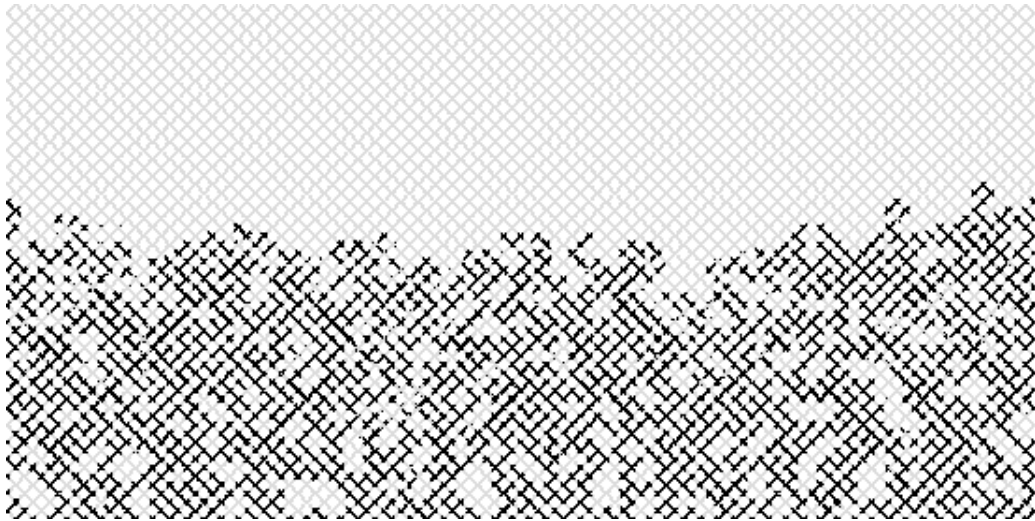


Figure 10

Aker et al.

Network Simulator for...

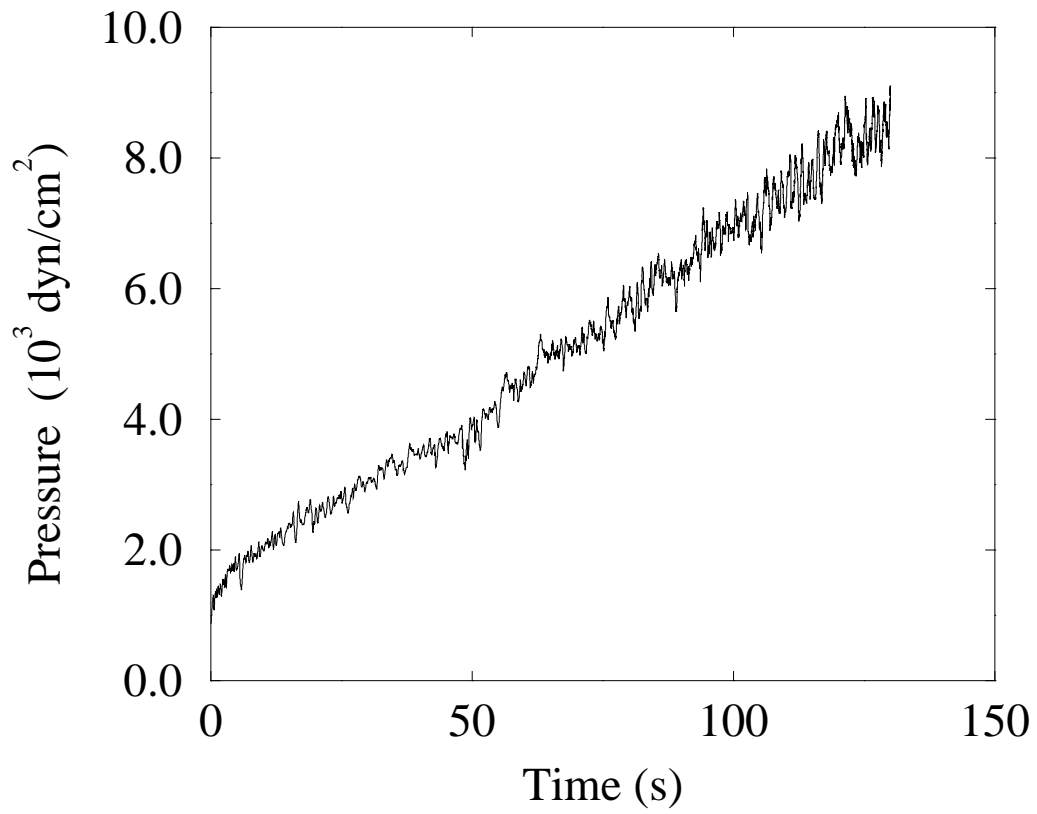


Figure 11

Aker et al.

Network Simulator for...

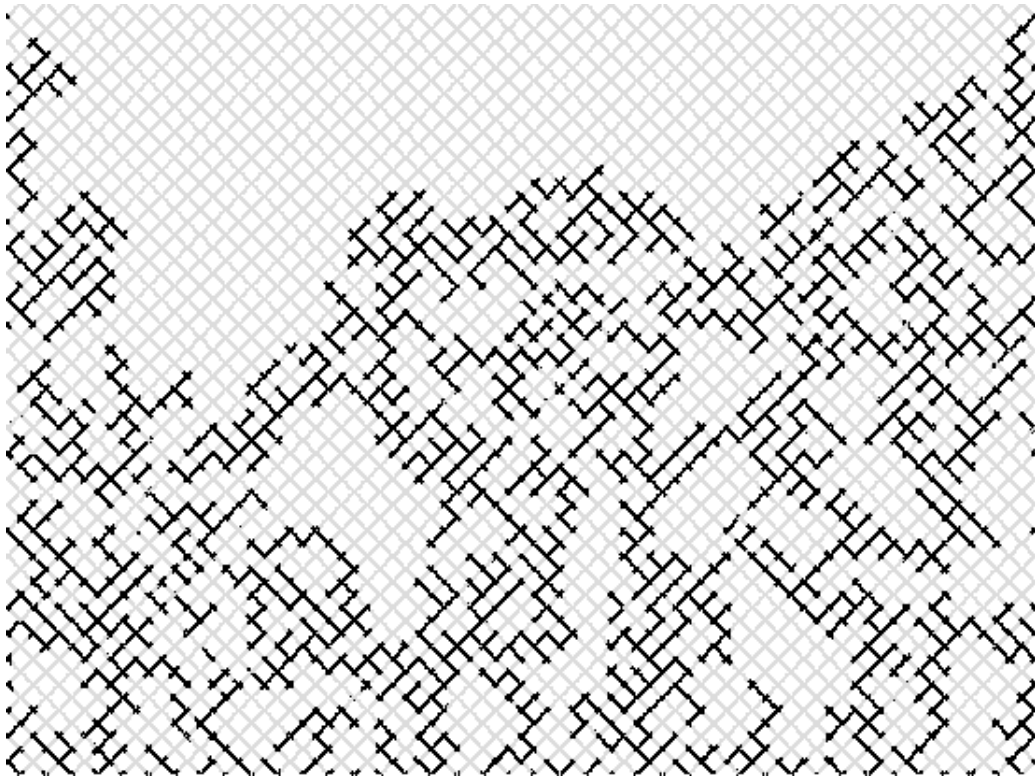


Figure 12

Aker et al.

Network Simulator for...

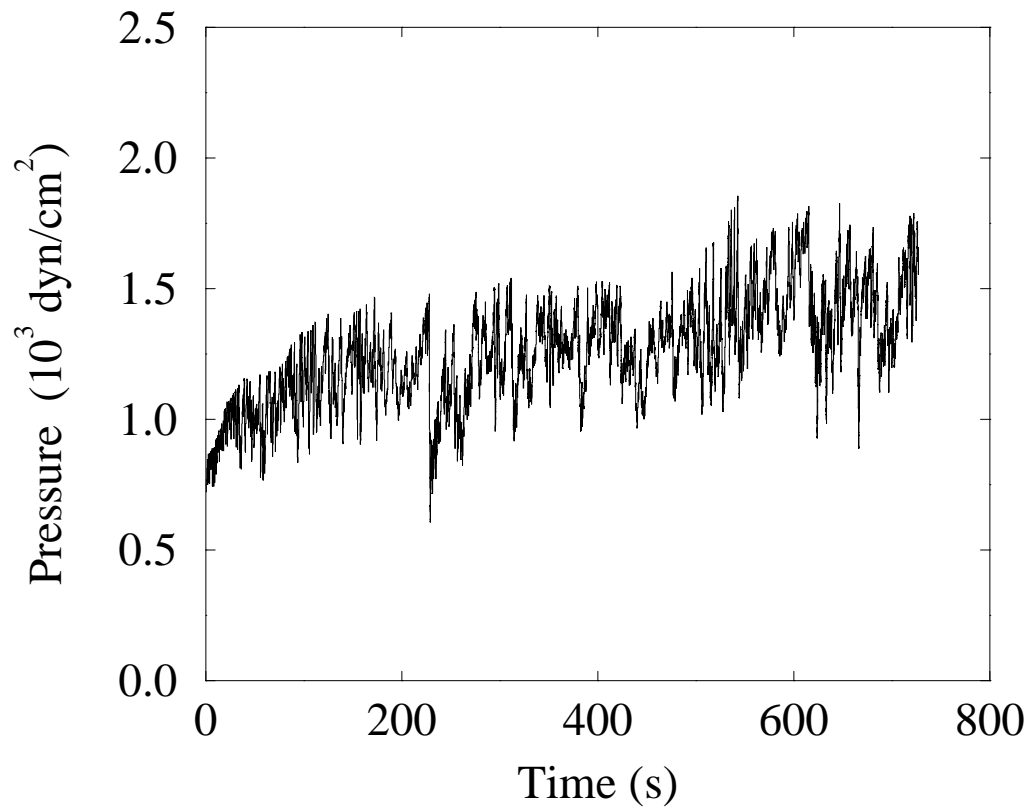


Figure 13

Aker et al.

Network Simulator for...

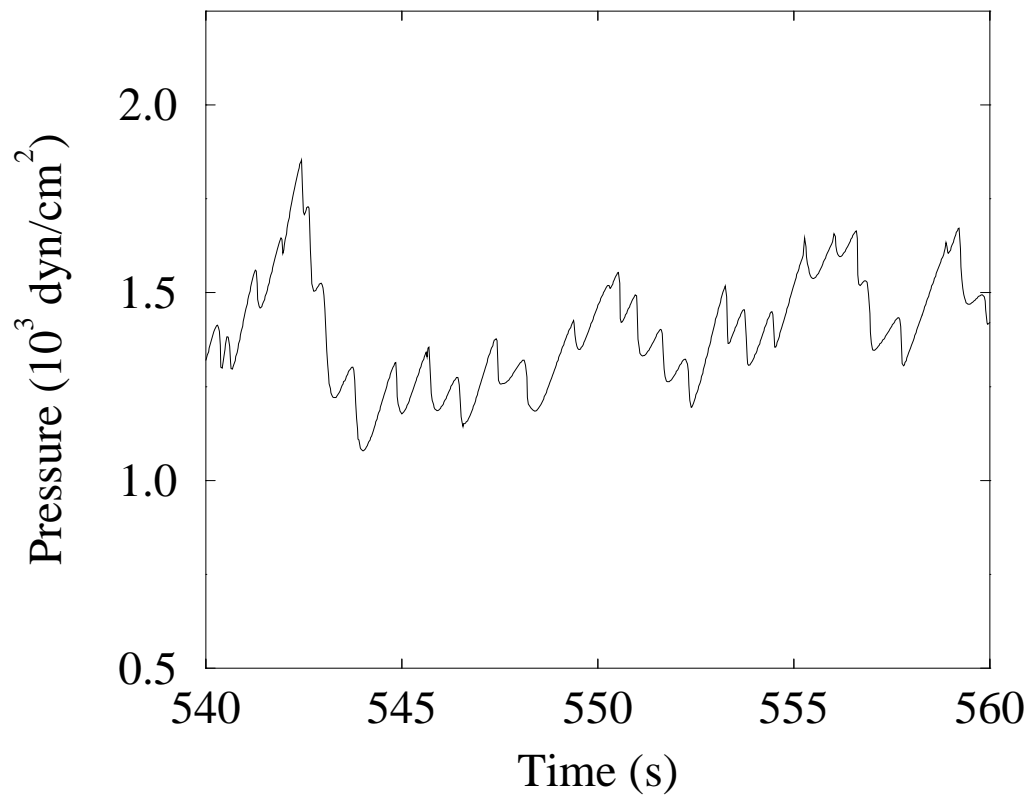


Figure 14

Aker et al.

Network Simulator for...